Digital Communications and Networks 10 (2024) 1804–1812

Contents lists available at ScienceDirect

Digital Communications and Networks

journal homepage: www.keaipublishing.com/dcan

Robust beamforming design for energy harvesting efficiency maximization in RIS-aided SWIPT system

Xingquan Li [a], Hongxia Zheng [b,*], Chunlong He [c,*], Xiaowen Tian [d], Xin Lin [e]

[a] School of Microelectronics, Shenzhen Institute of Information Technology, Shenzhen, 518000, China
[b] School of Electronic and Communication Engineering, Shenzhen Polytechnic University, Shenzhen, 518060, China
[c] Guangdong Key Laboratory of Intelligent Information Processing, Shenzhen University, Shenzhen, 518060, China
[d] College of Physics and Electromechanical Engineering, Jishou University, Hunan, 416000, China
[e] Institute of Artificial Intelligence and Blockchain, Guangzhou University, Guangzhou, 416000, China

ARTICLE INFO

Keywords:
Energy Harvesting Efficiency (EHE)
Reconfigurable Intelligent Surface (RIS)
Simultaneous Wireless Information and Power Transfer (SWIPT)
Imperfect Channel State Information (CSI)

ABSTRACT

This paper investigates Energy Harvesting Efficiency (EHE) maximization problems for Reconfigurable Intelligent Surface (RIS) aided Simultaneous Wireless Information and Power Transfer (SWIPT). This system focuses on the imperfect RIS-related channel and explores the robust beamforming design to maximize the EHE of all energy receivers while respecting the maximum transmit power of the Access Point (AP), RIS phase shift constraints, and maintaining a minimum signal-to-interference plus noise ratio for all information receivers under both linear and non-linear EH models. To solve these non-convex problem, the channel uncertainty related infinite constraints are approximated by using the S-procedure. With the introduction of slack variables, the transformed subproblems can be iteratively solved using alternating algorithm. Simulation results demonstrate that RIS is able to increase the system EHE.

1. Introduction

The new generation of industrial revolution has been quietly fought with the ever increasing of science and technology. To capture the apex of international manufacturing competition, the United States and Germany proposed the Advanced Manufacturing Partnership Program [1] and Industry 4.0 [2], respectively. To keep up with the international development, the Industrial Internet of Things (IIoT) was proposed, aiming to integrate the new generation of information and communication technologies to obtain much higher Spectral Efficiency (SE) and Energy Efficiency (EE) [3]. And IIoT as the core technology of the new generation of industrial revolution has brought unprecedented opportunities and challenges for the manufacturing industry [4]. As IIoT terminals continuously produce huge amounts of signals and data for sensing, control, data analysis and system maintenance, it causes great energy consumption, especially in some innovative IIoT systems such as smart grid [5], smart city [6], and e-health [7]. Given the limited resources of IIoT terminals [8], achieving efficient green communication is one of the key issues that hinder the development and commercialization of IIoT [9–11].

Simultaneous Wireless Information and Power Transfer (SWIPT) is one of the potential technologies to effectively prolong the work time and improve the communication quality of IIoT devices. It can operate Energy Harvesting (EH) as well as Information Transmitting (IT) from the intended signal, which is expected for the energy-hungry devices [12,13]. In [14], sum harvested energy maximization and EE maximization problems of Power-Splitting (PS) receivers have been investigated under linear and nonlinear EH models. Two pricing strategies have been proposed for D2D power allocation problem with the SWIPT PS scheme in [15]. Though SWIPT can effectively prolong the lifetime of IIoT devices, the EH and information transmitting still suffer from complex communication environments.

The development of new materials has led to the introduction of Reconfigurable Intelligent Surface (RIS), which has been considered as one of the potential techniques for the sixth-Generation (6G) wireless communication [16]. In a RIS, numerous passive reflecting elements are available that can independently adjust their phase shifts to properly reflect the intended signals to the target by establishing extra communication channels by a controller, achieving higher SE and EE than deployment of additional expensive power-hungry wireless communication facilities [17–19]. Some existing works have exploited RIS

* Corresponding authors.
E-mail addresses: 1950432012@email.szu.edu.cn (H. Zheng), hclong@szu.edu.cn (C. He).

https://doi.org/10.1016/j.dcan.2024.01.004
Received 15 February 2023; Received in revised form 22 December 2023; Accepted 22 January 2024
Available online 2 February 2024

to improve the performance of the wireless communication systems [20–23]. Specifically, [20] has investigated the performance of the system with the active and the passive RIS, demonstrating that the active RIS-aided communication system has better performance gain than that with the passive RIS. Authors in [21] have proposed a robust channel estimation algorithm based on variational Bayesian in the blocked RIS-aided multi-user communications to improve the performance of the millimeter-wave system. The system average bit error rate, average SE and outage probability have been analyzed in the RIS-aided multihop Full-Duplex (FD) relaying system [22]. A low-complexity channel estimation and passive beamforming for maximizing the achievable rate in RIS-assisted Multiple-Input Multiple-Output (MIMO) system with discrete phase shifts has been investigated in [23].

There are already some works that have improved the EH and IT process of the SWIPT through the RIS. For example, in [24], achievable data rate maximization problem has been discussed in IRS-assisted MIMO Orthogonal Frequency Division Multiplexing (OFDM) SWIPT system with nonlinear EH model. Simulation results have shown that the achievable data rate can be effectively improved by deploying RIS, especially when the number of the reflecting elements becomes larger. Authors in [25] have investigated the sum downlink and weighted uplink data rates by exploiting RIS-assisted Non-Orthogonal Multiple Access (NOMA) technology, demonstrating the effectiveness of improving the data rates by combining the RIS and NOMA. By exploiting active RIS, [26] has studied the weighted sum rate of Information Receivers (IRs) with linear EH model. Transmit power of the Access Point (AP) of the SWIPT system has been minimized via jointly optimizing its transmit beamforming and the reflect phase shifts of the IRSs under the Quality of Service (QoS) constraints in [27]. Moreover, the EE performance for the RIS-aided SWIPT has been studied in recent research [28–30]. Specifically, [28,29] studied the EE maximizing optimization problem in a secure RIS-aided SWIPT, and the numerical results revealed that EE initially increases and then decreases with the increase in the number of reflecting elements. Despite the utilization of the non-linear EH model, the traditional EE model still exhibits deficiencies in evaluating the EH process of Energy Receivers (ERs). [30] has introduced the EE indicator to measure the relationship between data rate and harvested energy in RIS-aided Multiple-Input Single-Output (MISO) SWIPT system by using the linear EH model, which is not suitable for the actual EH process of IIoTs.

However, the above works [26–28,30] merely use the traditional EE model to evaluate the harvesting energy of EH, which is not adequate to describe the energy acquisition more intuitively. Furthermore, the different EH models are vital due to the sensitivity to the energy for the IIoTs while the influence of the different EH models has been rarely discussed the existing works. In this paper, we introduce the Energy Harvesting Efficiency (EHE) [31–33] to describe EH more visually under linear and non-linear EH model in RIS-aided SWIPT. The system EHE maximization problems, both under linear and non-linear EH models, are optimized in the RIS-aided SWIPT by satisfying the maximum transmit power of the AP, the unit-modulus of the RIS's reflecting elements and the minimum Signal-to-Interference-Plus-Noise Ratio (SINR) demands of all the IRs. To address these optimization problems, an S-procedure is firstly used to reformulate the semi-infinite inequalities, followed by the adoption of an Alternate Optimization (AO) to obtain suboptimal solutions.

The rest of this paper is organized as follows. In Section 2, a RIS-aided SWIPT model, the linear and non-linear EH models for the ERs, the EHE model and the bounded CSI error for the RIS-related channels are presented. In Section 3, a robust design for the EHE maximization problems under linear and non-linear EH models is investigated with IRS-related channel uncertainty. In Section 4, the EHE performance of the proposed algorithms under different system parameters is evaluated through numerical simulations. We conclude the paper in Section 5.

Notations: Re{a} is the real part of the complex value a. Boldface upper case $\mathbf{H}$ and lower case $\mathbf{h}$ denote matrice $\mathbf{H}$ and vector $\mathbf{h}$, respectively. $\mathbb{C}^{N\times 1}$ is the set of $N\times 1$ complex vectors. $\|\mathbf{x}\|$ is the Euclidean norm of vector $\mathbf{x}$. $|y|$ is the norm of a complex number y, and $\|\mathbf{X}\|_F$ is the Frobenius norm of matrix $\mathbf{X}$. $(\cdot)^T$, $(\cdot)^*$, $(\cdot)^H$ represent the transpose, conjugate and Hermitian operators, respectively. $\mathbf{A}\odot\mathbf{B}$ is the Hadamard product of matrix $\mathbf{A}$ and matrix $\mathbf{B}$. Tr($\mathbf{A}$) denotes the trace operation of matrix $\mathbf{A}$. diag{$\cdot$} and arg{$\cdot$} are the diagonalization operation and extraction phase information operation, respectively. Notations that are used in this paper are illustrated in Table 1.

Table 1
List of notations.

Notation	Description
N	The antenna number of AP
M	The reflecting elements number of RIS
K_I, K_E	Number of IRs, ERs
$\mathbf{w}_i$, $\mathbf{v}_j$	Beamforming vectors for the ith IR, the jth ER
$\mathbf{h}_r$	The channel from AP to the ith IR
$\mathbf{h}_{r,i}$	The channel from RIS to the ith IR
$\mathbf{g}_j$	The channel from AP to the jth ER
$\mathbf{g}_{r,j}$	The channel from RIS to the jth ER
$\mathbf{H}$	The channel between AP and RIS
$\mathbf{\Phi}$	The diagonal reflection-coefficients matrix of the RIS
$\overline{\mathbf{H}}_i$, $\overline{\mathbf{G}}_j$	The RIS-related channel for the ith IR, the jth ER
$\widehat{\overline{\mathbf{H}}}_i$, $\widehat{\overline{\mathbf{G}}}_j$	The estimated channel of $\overline{\mathbf{H}}_i$, $\overline{\mathbf{G}}_j$
$\triangle\overline{\mathbf{H}}_i$, $\triangle\overline{\mathbf{G}}_j$	The CSI errors for $\overline{\mathbf{H}}_i$, $\overline{\mathbf{G}}_j$

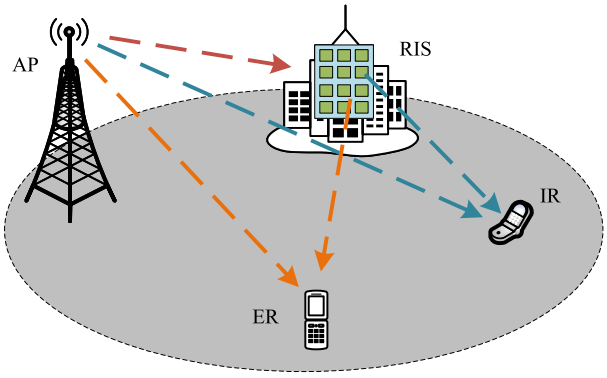

Fig. 1. RIS-aided SWIPT downlink communication system model.

2. System model

We consider a RIS-aided SWIPT downlink system with one AP, K_I IRs and K_E ERs and the system model is illustrated in Fig. 1. N and M are defined as the antennas number of AP and the number of reflecting elements of RIS, and $\mathcal{K}_\mathcal{I}=\{1,2,\cdots,K_I\}$, $\mathcal{K}_\mathcal{E}=\{1,2,\cdots,K_E\}$ and $\mathcal{M}=\{1,2,\cdots,M\}$ as the sets of IRs, ERs and reflecting elements, respectively. We assume IRs and ERs are equipped with single antenna.

When the SWIPT scheme is adopted, the AP transmits both information and energy signals to the IRs and the ERs simultaneously. In this paper, the information and the energy beamforming vectors are respectively denoted by $\mathbf{w}_i\in\mathbb{C}^{N\times 1}$ and $\mathbf{v}_j\in\mathbb{C}^{N\times 1}$, which are employed to realize IT and EH for the ith IR and the jth ER. Hence, the transmitted signal of AP can be modeled as

$$\mathbf{x}=\sum_{i\in\mathcal{K}_\mathcal{I}}\mathbf{w}_i s_i^I+\sum_{j\in\mathcal{K}_\mathcal{E}}\mathbf{v}_j s_j^E \tag{1}$$

where s_i^I and s_j^E are the information bearing and energy carrying signals of the ith IR and the jth ER, respectively. We assume that they obey $s_i^I\sim\mathcal{CN}(0,1)$, $s_j^E\sim\mathcal{CN}(0,1)$ and $\mathbb{E}\left\{|s_i^I|^2\right\}=\mathbb{E}\left\{|s_j^E|^2\right\}=1,\forall i\in\mathcal{K}_\mathcal{I},\forall j\in\mathcal{K}_\mathcal{E}$.

Hence, the received signal of the ith IR can be expressed as

$$y_i^I=\left(\mathbf{h}_i^H+\mathbf{h}_{r,i}^H\mathbf{\Phi}\mathbf{H}\right)\mathbf{x}+n_i$$

$$= \widetilde{\mathbf{h}}_i^H \mathbf{w}_i s_i^I + \sum_{k \in \mathcal{K}_\mathcal{I} \setminus \{i\}} \widetilde{\mathbf{h}}_i^H \mathbf{w}_k s_k^I + \sum_{j \in \mathcal{K}_\mathcal{I}} \widetilde{\mathbf{h}}_i^H \mathbf{v}_j s_j^E + n_i \tag{2}$$

where $\widetilde{\mathbf{h}}_i^H = \mathbf{h}_i^H + \mathbf{h}_{r,i}^H \mathbf{\Phi} \mathbf{H}$, $\mathbf{h}_i \in \mathbb{C}^{N\times 1}$ and $\mathbf{h}_{r,i} \in \mathbb{C}^{M\times 1}$ are the direct communication channel from AP and RIS to the ith IR, respectively. $\mathbf{H} \in \mathbb{C}^{M\times N}$ is the communication channel matrix between AP and RIS. $\mathbf{\Phi} = \mathrm{diag}\{e^{j\theta_1}, \cdots, e^{j\theta_2}, \cdots, e^{j\theta_M}\}$ is the diagonal reflection-coefficients matrix, in which the phase shift of the ith reflection element of the RIS is denoted by $\theta_i \in [0, 2\pi]$. $n_i \sim \mathcal{CN}(0, \sigma_i^2), \forall i \in \mathcal{K}_\mathcal{I}$ is the additive white Gaussian noise at the ith IR.

Therefore, according to (2), the SINR of the ith IR can be modeled as

$$SINR_i = \frac{|\widetilde{\mathbf{h}}_i^H \mathbf{w}_i|^2}{\sum\limits_{k \in \mathcal{K}_\mathcal{I} \setminus \{i\}} |\widetilde{\mathbf{h}}_i^H \mathbf{w}_k|^2 + \sum\limits_{j \in \mathcal{K}_\mathcal{E}} |\widetilde{\mathbf{h}}_i^H \mathbf{v}_j|^2 + \sigma_i^2} \tag{3}$$

Similarly, the received signal of the jth ER is given as

$$\begin{aligned} y_j^E &= \left(\mathbf{g}_j^H + \mathbf{g}_{r,j}^H \mathbf{\Phi} \mathbf{H}\right) \mathbf{x} + n_j \\ &= \sum_{i \in \mathcal{K}_\mathcal{I}} \widetilde{\mathbf{g}}_j^H \mathbf{w}_i s_i^I + \sum_{l \in \mathcal{K}_\mathcal{E}} \widetilde{\mathbf{g}}_j^H \mathbf{v}_l s_l^E + n_j \end{aligned} \tag{4}$$

where $\widetilde{\mathbf{g}}_j^H = \mathbf{g}_j^H + \mathbf{g}_{r,j}^H \mathbf{\Phi} \mathbf{H}$, $\mathbf{g}_j \in \mathbb{C}^{N\times 1}$ and $\mathbf{g}_{r,j} \in \mathbb{C}^{M\times 1}$ denote the direct communication channel from AP and RIS to the jth ER, respectively. $n_j \sim \mathcal{CN}(0, \sigma_j^2), \forall j \in \mathcal{K}_\mathcal{E}$ is the additive white Gaussian noise at the jth ER.

When the linear EH model is used for all ERs, the harvested energy of the jth ER can be formulated as

$$E_j^L = \tau_j P_j^L \tag{5}$$

where $\tau_j \in (0, 1)$ is a constant that denotes the power conversion efficiency of the jth ER. P_j^L is the averaged harvested power for the jth ER, which can be defined as

$$P_j^L \triangleq \mathbb{E}\left\{|y_j^E|^2\right\} = \sum_{i \in \mathcal{K}_\mathcal{I}} |\widetilde{\mathbf{g}}_j^H \mathbf{w}_i s_i^I|^2 + \sum_{l \in \mathcal{K}_\mathcal{E}} |\widetilde{\mathbf{g}}_j^H \mathbf{v}_l s_l^E|^2 \tag{6}$$

However, the ideal linear EH model cannot effectively measure the characteristics of the realistic non-linear EH circuits. To comply with the reality, a practical non-linear EH model investigated in [14] is also concerned. After using the non-linear EH model, the harvested energy of the jth ER is expressed as

$$E_j^N = \frac{f_j^p - M_j \Omega_j}{1 - \Omega_j}, \Omega_j = \frac{1}{1 + e^{a_j b_j}} \tag{7}$$

where $f_j^p = \frac{M_j}{1+e^{-a_j(P_j^L - b_j)}}$, E_j^N is the total harvested energy of the jth ER, f_j^p is expressed as the conventional logistic function for the received power P_j^L of the jth ER. M_j, a_k and b_k represent constants that are related to the joint effects of various non-linear characteristics caused by the hardware facilities. These constraints can be easily obtained using standard curve fitting tools.

2.1. Channel uncertainty and CSI error model

It is readily seen that there are two kinds of communication channels in the RIS-aided wireless communication systems. Specifically, the direct and the reflecting related channels from AP to the ith IR and the jth ER, are respectively denoted by $\mathbf{h}_i$, $\mathbf{g}_j$, and $\overline{\mathbf{H}}_i = \mathrm{diag}(\mathbf{h}_{r,i}^H)\mathbf{H}$, $\overline{\mathbf{G}}_j = \mathrm{diag}(\mathbf{g}_{r,j}^H)\mathbf{H}$. Hence, the performance of the RIS-aided communication system depends on the CSI of these communication channels. The channel quantization error can be approximated in a bounded region [34,35]. Here, we use the bounded CSI error model to represent the RIS-related channel uncertainty.

2.1.1. RIS-related channel uncertainty

Due to the passive characteristics of RIS, it is difficult to obtain the perfect CSI for RIS-related communication channels. In this paper, we take the imperfect CSI of RIS-related channels into consideration. Therefore, the RIS-related channel $\overline{\mathbf{H}}_i$ and $\overline{\mathbf{G}}_j$ with CSI errors can be respectively modeled as

$$\overline{\mathbf{H}}_i = \widehat{\overline{\mathbf{H}}}_i + \triangle \overline{\mathbf{H}}_i, i \in \mathcal{K}_\mathcal{I} \tag{8}$$

$$\overline{\mathbf{G}}_j = \widehat{\overline{\mathbf{G}}}_j + \triangle \overline{\mathbf{G}}_j, j \in \mathcal{K}_\mathcal{E} \tag{9}$$

where $\widehat{\overline{\mathbf{H}}}_i$ and $\widehat{\overline{\mathbf{G}}}_j$ denote the estimated channel for $\overline{\mathbf{H}}_i$ and $\overline{\mathbf{G}}_j$, which can be obtained by traditional channel estimating methods at the AP. $\triangle \overline{\mathbf{H}}_i$ and $\triangle \overline{\mathbf{G}}_j$ are the uncertain CSI errors for different communication channels.

2.1.2. Bounded CSI error model

To evaluate the channel quantization error for the RIS-related channels, the bounded CSI error model is introduced and can be formulated as

$$\| \triangle \overline{\mathbf{H}}_i \|_F \le \varepsilon_{r,i}^I, i \in \mathcal{K}_\mathcal{I}, \| \triangle \overline{\mathbf{G}}_j \|_F \le \varepsilon_{r,j}^E, j \in \mathcal{K}_\mathcal{E} \tag{10}$$

where $\varepsilon_{r,i}^I$ and $\varepsilon_{r,j}^E$ denote the radii of the uncertain region for the different CSI errors already known for AP, which is appropriate for describing the channel quantization error [34].

2.1.3. EHE model

To analyze the energy absorption efficiency more directly for all the ERs, we aim to maximize the EHE of all ERs with respect to optimizing the beamforming vectors of AP and the phase shifts of RIS. According to the existing works [31,32], the sum EHE of all ERs can be modeled as

$$EHE = \frac{\sum\limits_{j \in \mathcal{K}_\mathcal{E}} E_j}{P_{total}} \tag{11}$$

where $E_j = E_j^L$ when the jth ER adopts the linear EH model in the EH process, otherwise $E_j = E_j^N$. P_{total} is the total power consumption of AP, which can be written as

$$P_{total} = \sum_{i \in \mathcal{K}_\mathcal{I}} \|\mathbf{w}_i\|^2 + \sum_{l \in \mathcal{K}_\mathcal{E}} \|\mathbf{v}_l\|^2 + P_c \tag{12}$$

where P_c is the hardware circuits consumption power of AP such as the frequency synthesizers digital-to-analog converters [32].

3. Robust beamforming design

In this paper, the optimization problems for maximizing the sum EHE of all ERs are studied under the case that RIS-related communication channels are composed by the estimated CSI and the bounded CSI errors. Both the linear and non-linear EH models at ERs are concerned in the optimization problem and the solving process is presented.

3.1. Problem formulation

Our goal is to maximize the total EHE of all ERs as well as satisfying the minimum SINR constraint for each IR, the maximum transmit power limit of AP and the phase shifts requirements of the RIS. After defining $\mathcal{E}_i^I \triangleq \{\forall \| \triangle \overline{\mathbf{H}}_i \|_F \le \varepsilon_{r,i}^I\}$ and $\mathcal{E}_j^E \triangleq \{\forall \| \triangle \overline{\mathbf{G}}_j \|_F \le \varepsilon_{r,j}^E\}$, for the linear EH model, we can formulate the optimization problem as

$$\mathcal{P}_1 \quad \max_{\{\mathbf{w_i}\},\{\mathbf{v_j}\},\mathbf{\Phi}} \frac{\sum\limits_{j \in \mathcal{K}_\mathcal{E}} \tau_j \left(\sum\limits_{i \in \mathcal{K}_\mathcal{I}} \mathbf{w}_i^H \widetilde{\mathbf{G}}_j^H \mathbf{w}_i + \sum\limits_{l \in \mathcal{K}_\mathcal{E}} \mathbf{v}_l^H \widetilde{\mathbf{G}}_j^H \mathbf{v}_l \right)}{\sum\limits_{i \in \mathcal{K}_\mathcal{I}} \|\mathbf{w}_i\|^2 + \sum\limits_{l \in \mathcal{K}_\mathcal{E}} \|\mathbf{v}_l\|^2 + P_c} \tag{13a}$$

$$\text{s.t.} \quad \sum_{i\in\mathcal{K}_\mathcal{I}} \|\mathbf{w}_i\|^2 + \sum_{l\in\mathcal{K}_\mathcal{E}} \|\mathbf{v}_l\|^2 \le P_{max} \tag{13b}$$

$$SINR_i \ge \gamma_{min}, \mathcal{E}_i^I, i \in \mathcal{K}_\mathcal{I} \tag{13c}$$

$$0 \le \theta_m \le 2\pi, m \in \mathcal{M} \tag{13d}$$

where $\widetilde{\mathbf{G}}_j = \widetilde{\mathbf{g}}_j \widetilde{\mathbf{g}}_j^H$, P_{max} is the maximum transmit power available at AP. γ_{min} denotes the minimum SINR requirement of IRs.

Similarly, when all the ERs use non-linear EH model in the EH process, the EHE maximization optimization problem can be modeled as

$$\mathcal{P}_2 \quad \max_{\{\mathbf{w_i}\},\{\mathbf{v_j}\},\mathbf{\Phi}} \quad \frac{\sum_{j\in\mathcal{K}_\mathcal{E}} \left(\frac{1}{1+e^{-a_j(P_j^L - b_j)}} - \Omega_j \right) \frac{M_j}{1-\Omega_j}}{\sum_{i\in\mathcal{K}_\mathcal{I}} \|\mathbf{w}_i\|^2 + \sum_{l\in\mathcal{K}_\mathcal{E}} \|\mathbf{v}_l\|^2 + P_c} \tag{14a}$$

$$\text{s.t.} \quad \text{(13b)} \sim \text{(13d)} \tag{14b}$$

3.2. Robust beamforming design with linear EH model

The objective function and the constraints (13c) in Problem $\mathcal{P}_1$ are non-convex due to the coupled variables and the RIS-related CSI errors. To deal with it, we firstly introduce the slack variable η_1 to equivalently transform this problem into

$$\mathcal{P}_{1-1} \quad \max_{\{\mathbf{w_i}\},\{\mathbf{v_j}\},\mathbf{\Phi},\eta_1} \quad \eta_1 \tag{15a}$$

$$\text{s.t.} \quad \frac{\sum_{j\in\mathcal{K}_\mathcal{E}} \tau_j \left(\sum_{i\in\mathcal{K}_\mathcal{I}} \mathbf{w}_i^H \widetilde{\mathbf{G}}_j^H \mathbf{w}_i + \sum_{l\in\mathcal{K}_\mathcal{E}} \mathbf{v}_l^H \widetilde{\mathbf{G}}_j^H \mathbf{v}_l \right)}{\sum_{i\in\mathcal{K}_\mathcal{I}} \|\mathbf{w}_i\|^2 + \sum_{l\in\mathcal{K}_\mathcal{E}} \|\mathbf{v}_l\|^2 + P_c} \ge \eta_1 \tag{15b}$$

$$\text{(13b)} \sim \text{(13d)} \tag{15c}$$

Then, according to $\widetilde{\mathbf{G}}_j = \widetilde{\mathbf{g}}_j \widetilde{\mathbf{g}}_j^H$, $\widetilde{\mathbf{g}}_j^H = \mathbf{g}_j^H + \mathbf{g}_{r,j}^H \mathbf{\Phi} \mathbf{H}$ and (9), constraint (15b) can be further transformed into

$$\sum_{j\in\mathcal{K}_\mathcal{E}} \tau_j \left[C_{1,j} + 2\text{Re}\left\{ \text{Tr}(\mathbf{A}_{1,j} \triangle \overline{\mathbf{G}}_j) \right\} + \boldsymbol{\phi}^{\text{H}} \triangle \overline{\mathbf{G}}_{\text{j}} \mathbf{B}_1 \triangle \overline{\mathbf{G}}_{\text{j}}^{\text{H}} \boldsymbol{\phi} \right] \ge \eta_1 \left(\sum_{i\in\mathcal{K}_\mathcal{I}} \|\mathbf{w}_i\|^2 + \sum_{l\in\mathcal{K}_\mathcal{E}} \|\mathbf{v}_l\|^2 + P_c \right) \tag{16}$$

where $\mathbf{W}_i = \mathbf{w}_i \mathbf{w}_i^H$, $\mathbf{V}_l = \mathbf{v}_l \mathbf{v}_l^H$, $\mathbf{B}_1 = \sum_{i\in\mathcal{K}_\mathcal{I}} \mathbf{W}_i + \sum_{l\in\mathcal{K}_\mathcal{E}} \mathbf{V}_l$, $C_{1,j} = \text{Tr}\left(\mathbf{g}_{\text{j}} \mathbf{g}_{\text{j}}^{\text{H}} \mathbf{B}_1\right) + 2\text{Re}\left\{ \text{Tr}\left(\mathbf{g}_{\text{j}} \boldsymbol{\phi}^{\text{H}} \widehat{\overline{\mathbf{G}}}_{\text{j}} \mathbf{B}_1 \right) \right\} + \text{Tr}\left(\widehat{\overline{\mathbf{G}}}_{\text{j}}^{\text{H}} \boldsymbol{\phi}\boldsymbol{\phi}^{\text{H}} \widehat{\overline{\mathbf{G}}}_{\text{j}} \mathbf{B}_1 \right)$, and $\mathbf{A}_{1,j} = \mathbf{B}_1 (\mathbf{g}_j \boldsymbol{\phi}^H + \widehat{\overline{\mathbf{G}}}_j^H \boldsymbol{\phi}\boldsymbol{\phi}^H)$.

By using $\mathbf{a}^H \mathbf{X} \mathbf{B} \mathbf{X}^H \mathbf{c} = \text{vec}(\mathbf{X})^{\text{H}} (\text{B} \otimes \mathbf{ca}^{\text{H}}) \text{vec}(\mathbf{X})$, $\text{Tr}(\mathbf{A}^{\text{H}}\mathbf{B}) = \text{vec}(\mathbf{A})^{\text{H}} \text{vec}(\mathbf{B})$ and $C_2 = \sum_{i\in\mathcal{K}_\mathcal{I}} \|\mathbf{w}_i\|^2 + \sum_{l\in\mathcal{K}_\mathcal{E}} \|\mathbf{v}_l\|^2 + P_c$. (16) can be simplified into

$$\sum_{j\in\mathcal{K}_\mathcal{E}} \tau_j \left[\text{vec}(\triangle \overline{\mathbf{G}}_{\text{j}})^{\text{H}} (\mathbf{B}_1 \otimes \boldsymbol{\phi}\boldsymbol{\phi}^{\text{H}}) \text{vec}(\triangle \overline{\mathbf{G}}_{\text{j}}) + 2\text{Re}\left\{ \text{vec}(\mathbf{A}_{1,\text{j}}^{\text{H}})^{\text{H}} \text{vec}(\triangle \overline{\mathbf{G}}_{\text{j}}) \right\} + \text{C}_{1,\text{j}} - \frac{\eta_1 \text{C}_2}{\tau_{\text{j}} \text{K}_{\text{E}}} \right] \ge 0 \tag{17}$$

This constraint remains non-convex because it contains unlimited CSI errors, which are brought by the RIS-related channels. Nevertheless, we can approximate it into Linear Matrix Inequations (LMIs) by exploiting the following Lemma [34,36,37].

Lemma 1. *Define the following quadratic functions of the variable* $\mathbf{x} \in \mathbb{C}^{N\times 1}$*:*

$$f_k(\mathbf{x}) = \mathbf{x}^H \mathbf{T}_k \mathbf{x} + 2\text{Re}\{\mathbf{s}_{\text{k}}^{\text{T}} \mathbf{x}\} + \text{v}_{\text{k}}, \text{k} \in [0, \text{P}]$$

where $\mathbf{T}_k = \mathbf{T}_k^H$*, the condition* $f_k(\mathbf{x}) \ge 0, k \in [0, P] \Rightarrow f_0(\mathbf{x})$ *holds if and only if there exists* $\omega_k \ge 0, k \in [0, P]$ *that satisfies*

$$\begin{bmatrix} \mathbf{T}_0 & \mathbf{s}_0 \\ \mathbf{s}_0^T & v_0 \end{bmatrix} - \sum_{k=1}^{P} \omega_k \begin{bmatrix} \mathbf{T}_k & \mathbf{s}_k \\ \mathbf{s}_k^T & v_k \end{bmatrix} \succeq 0$$

Because the EHE of each ER is positive, the channel uncertainty in (17) can be approximated according to Lemma 1 and the parameters in Lemma 1 for the jth ER is formulated as

$$P = 1, \mathbf{T}_0 = \mathbf{B}_1 \otimes \boldsymbol{\phi}\boldsymbol{\phi}^H, \mathbf{s}_0 = \text{vec}(\mathbf{A}_{1,\text{j}}^{\text{H}}), \mathbf{x} = \text{vec}(\triangle \overline{\mathbf{G}}_{\text{j}})$$

$$v_0 = C_{1,j} - \frac{\eta_1}{\tau_j K_E} \left(\sum_{i\in\mathcal{K}_\mathcal{I}} \|\mathbf{w}_i\|^2 + \sum_{l\in\mathcal{K}_\mathcal{E}} \|\mathbf{v}_l\|^2 + P_c \right)$$

$$\mathbf{T}_1 = -\mathbf{I}, v_1 = \frac{(\varepsilon_{r,j}^E)^2}{K_E}$$

Then, (17) can be transformed into its approximate LMIs as follows:

$$\tau_j \begin{bmatrix} \mathbf{T}_0 + \omega_j \mathbf{I} & \mathbf{s}_j \\ \mathbf{s}_j^T & \widehat{C}_{1,j} \end{bmatrix} \succeq 0, j \in \mathcal{K}_\mathcal{E} \tag{18}$$

where $\boldsymbol{\omega} = [\omega_1, \cdots, \omega_{K_E}] \ge 0$ is the introduced slack variable, $\widehat{C}_{1,j} = C_{1,j} - \frac{\eta_1 C_2}{\tau_j K_E} - \frac{\omega_j (\varepsilon_{r,j}^E)^2}{K_E}$.

Next, we deal with the QoS requirement constraints (13c). According to (3), we have

$$\begin{aligned} &\text{Tr}\left[\left((1+\gamma_{\text{min}}) \mathbf{W}_{\text{i}} - \gamma_{\text{min}} \mathbf{B}_1 \right) \mathbf{C}_3 \right] \\ &+ 2\text{Re}\left\{ Tr[\left((1+\gamma_{min}) \mathbf{W}_i - \gamma_{min} \mathbf{B}_1 \right) \mathbf{A}_{2,i} \triangle \overline{\mathbf{H}}_i] \right\} \\ &+ \boldsymbol{\phi}^H \triangle \overline{\mathbf{H}}_i \left((1+\gamma_{min}) \mathbf{W}_i - \gamma_{min} \mathbf{B}_1 \right) \triangle \overline{\mathbf{H}}_i^H \boldsymbol{\phi} \\ &- \gamma_{min} \sigma_i^2 \ge 0, \mathcal{E}_i^I, i \in \mathcal{K}_\mathcal{I} \end{aligned} \tag{19}$$

where $\mathbf{C}_{3,i} = \mathbf{h}_i \mathbf{h}_i^H + 2\text{Re}\left\{ \mathbf{h}_i \boldsymbol{\phi}^H \widehat{\overline{\mathbf{H}}}_i \right\} + \widehat{\overline{\mathbf{H}}}_i^H \boldsymbol{\phi}\boldsymbol{\phi}^H \widehat{\overline{\mathbf{H}}}_i$, $\mathbf{A}_{2,i} = \mathbf{h}_i \boldsymbol{\phi}^H + \widehat{\overline{\mathbf{H}}}_i^H \boldsymbol{\phi}\boldsymbol{\phi}^H$.

Defining $\overline{\mathbf{B}}_i = (1+\gamma_{min}) \mathbf{W}_i - \gamma_{min} \mathbf{B}_1$, constraint (19) can be further transformed into

$$\begin{aligned} &\text{vec}(\triangle \overline{\mathbf{H}}_{\text{i}})^{\text{H}} (\overline{\mathbf{B}}_{\text{i}} \otimes \boldsymbol{\phi}\boldsymbol{\phi}^{\text{H}}) \text{vec}(\triangle \overline{\mathbf{H}}_{\text{i}}) \\ &+ 2\text{Re}\left\{ \text{vec}\left(\mathbf{A}_{2,\text{i}}^{\text{H}} \overline{\mathbf{B}}_{\text{i}}^{\text{H}} \right)^{\text{H}} \text{vec}(\triangle \overline{\mathbf{H}}_{\text{i}}) \right\} \\ &+ \text{Tr}[\overline{\mathbf{B}}_{\text{i}} \mathbf{C}_{3,\text{i}}] - \gamma_{\text{min}} \sigma_{\text{i}}^2 \ge 0, \mathcal{E}_{\text{i}}^{\text{I}}, \text{i} \in \mathcal{K}_\mathcal{I} \end{aligned} \tag{20}$$

Similarly, by exploiting Lemma 1, constraints (20) can also be reformulated as

$$\begin{bmatrix} \hat{\mathbf{T}}_{1,i} + \hat{\omega}_i \mathbf{I} & \mathbf{t}_i \\ \mathbf{t}_i^T & C_{4,i} \end{bmatrix} \succeq 0, i \in \mathcal{K}_\mathcal{I} \tag{21}$$

where $\hat{\boldsymbol{\omega}} = [\hat{\omega}_1, \cdots, \hat{\omega}_{K_I}]$ is the introduced slack variable, $\hat{\mathbf{T}}_{1,i} = \overline{\mathbf{B}}_i \otimes \boldsymbol{\phi}\boldsymbol{\phi}^H$, $\mathbf{t}_i = \text{vec}\left(\mathbf{A}_{2,\text{i}}^{\text{H}} \overline{\mathbf{B}}_{\text{i}}^{\text{H}} \right)$, $C_{4,i} = \text{Tr}[\overline{\mathbf{B}}_{\text{i}} \mathbf{C}_{3,\text{i}}] - \gamma_{\text{min}} \sigma_{\text{i}}^2 - \hat{\omega}_{\text{i}} (\varepsilon_{\text{r,i}}^{\text{I}})^2$.

After the above conversion, Problem $\mathcal{P}_{1-1}$ can be approximately reformulated as the following optimization problem

$$\mathcal{P}_{1-2} \quad \max_{\{\mathbf{w_i}\},\{\mathbf{v_j}\},\mathbf{\Phi},\eta_1,\boldsymbol{\omega},\hat{\boldsymbol{\omega}}} \quad \eta_1 \tag{22a}$$

$$\text{s.t.} \quad \text{(13b)}, \text{(13d)}, \text{(18)}, \text{(21)} \tag{22b}$$

$$\boldsymbol{\omega} \ge 0, \hat{\boldsymbol{\omega}} \ge 0 \tag{22c}$$

This problem is a non-convex feasibility-check problem with the coupled variables in constraints (22b). Next, the alternate optimization method is adopted to alternatively optimize these variables.

3.2.1. Optimizing beamforming vectors $\{\mathbf{w_i}\},\{\mathbf{v_j}\}$ with fixed phase shift matrix $\mathbf{\Phi}$

With fixed phase shift matrix $\mathbf{\Phi}$, Problem $\mathcal{P}_{1-2}$ is reformulated as

$$\mathcal{P}_{1-3-1} \quad \max_{\{\mathbf{w_i}\},\{\mathbf{v_j}\},\eta_1,\boldsymbol{\omega},\hat{\boldsymbol{\omega}}} \quad \eta_1 \tag{23a}$$

$$\text{s.t.} \quad (13\text{b}),(18),(21),(22\text{c}) \tag{23b}$$

According to (15b), it is easy to know that the optimal η_1^* can be obtained as long as obtaining the optimal solutions of $\{\mathbf{w_i^*}\},\{\mathbf{v_j^*}\}$. Hence, Problem $\mathcal{P}_{1-3-1}$ can be transformed into the following feasibility-check problem with fixed η_1.

$$\mathcal{P}_{1-3-2} \quad \max_{\{\mathbf{w_i}\},\{\mathbf{v_j}\},\boldsymbol{\omega},\hat{\boldsymbol{\omega}}} \quad \eta_1, \quad s.t. \quad (23\text{b}) \tag{24a}$$

To make this feasibility-check problem more trackable, slack variables α and $\boldsymbol{\beta}=[\beta_1,\cdots,\beta_{K_I}]$ are introduced. Then, Problem $\mathcal{P}_{1-3-2}$ can be modified as

$$\mathcal{P}_{1-3-3} \quad \max_{\{\mathbf{w_i}\},\{\mathbf{v_j}\},\boldsymbol{\omega},\hat{\boldsymbol{\omega}},\alpha,\boldsymbol{\beta}} \quad \sum_{j\in\mathcal{K}_\mathcal{E}}\alpha_j+\sum_{i\in\mathcal{K}_\mathcal{I}}\beta_i \tag{25a}$$

$$\text{s.t. } \tau_j\begin{bmatrix}\mathbf{T}+\omega_j\mathbf{I} & \mathbf{s}_j\\ \mathbf{s}_j^T & \widehat{C}_{1,j}-\alpha_j\end{bmatrix}\succeq 0, j\in\mathcal{K}_\mathcal{E} \tag{25b}$$

$$\begin{bmatrix}\hat{\mathbf{T}}_{1,i}+\hat{\omega}_i\mathbf{I} & \mathbf{t}_i\\ \mathbf{t}_i^T & C_{4,i}-\beta_i\end{bmatrix}\succeq 0, i\in\mathcal{K}_\mathcal{I} \tag{25c}$$

$$(13\text{b}),(22\text{c}) \tag{25d}$$

This problem is a second-order cone programming (SOCP) for $\{\mathbf{w_i}\}$ and $\{\mathbf{v_j}\}$, which can be solved by using CVX.

3.2.2. Optimizing phase shift vector $\boldsymbol{\phi}$ with fixed beamforming vectors $\{\mathbf{w_i}\},\{\mathbf{v_j}\}$

Given $\{\mathbf{w_i}\},\{\mathbf{v_j}\}$, Problem $\mathcal{P}_{1-2}$ is simplified as a feasibility-check subproblem for $\boldsymbol{\phi}$, which can be formulated as

$$\mathcal{P}_{1-4-1} \quad \max_{\boldsymbol{\phi},\boldsymbol{\omega},\hat{\boldsymbol{\omega}},\alpha,\boldsymbol{\beta}} \quad \sum_{j\in\mathcal{K}_\mathcal{E}}\alpha_j+\sum_{i\in\mathcal{K}_\mathcal{I}}\beta_i \tag{26a}$$

$$\text{s.t. } \tau_j\begin{bmatrix}\mathbf{T}+\omega_j\mathbf{I} & \mathbf{s}_j\\ \mathbf{s}_j^T & \widehat{C}_{1,j}-\alpha_j\end{bmatrix}\succeq 0, j\in\mathcal{K}_\mathcal{E} \tag{26b}$$

$$\begin{bmatrix}\hat{\mathbf{T}}_{1,i}+\hat{\omega}_i\mathbf{I} & \mathbf{t}_i\\ \mathbf{t}_i^T & C_{4,i}-\beta_i\end{bmatrix}\succeq 0, i\in\mathcal{K}_\mathcal{I} \tag{26c}$$

$$(13\text{d}),(22\text{c}) \tag{26d}$$

Problem $\mathcal{P}_{1-4-1}$ is still non-convex and challenging to solve due to the quadratic form of $\boldsymbol{\phi}$ in constraints (26b) and (26c). But the quadratic form of variables can be approximated as its lower bounds according to the following Lemma.

Lemma 2. *Let $\boldsymbol{\phi}^{(t)}$ be the optimal value for $\boldsymbol{\phi}$ at the tth iteration, then we have*

$$\boldsymbol{\phi}\boldsymbol{\phi}^H\succeq\boldsymbol{\phi}\boldsymbol{\phi}^{(t)H}+\boldsymbol{\phi}^{(t)}\boldsymbol{\phi}^H-\boldsymbol{\phi}^{(t)}\boldsymbol{\phi}^{(t)H}$$

Proof. According to the above discussion, we have the following inequalities

$$(\boldsymbol{\phi}-\boldsymbol{\phi}^{(t)})(\boldsymbol{\phi}-\boldsymbol{\phi}^{(t)})^H\succeq\mathbf{0}$$

$$\Rightarrow\boldsymbol{\phi}\boldsymbol{\phi}^H-\boldsymbol{\phi}\boldsymbol{\phi}^{(t)H}-\boldsymbol{\phi}^{(t)}\boldsymbol{\phi}^H+\boldsymbol{\phi}^{(t)}\boldsymbol{\phi}^{(t)H}\succeq\mathbf{0}.$$

$$\Rightarrow\boldsymbol{\phi}\boldsymbol{\phi}^H\succeq\boldsymbol{\phi}\boldsymbol{\phi}^{(t)H}+\boldsymbol{\phi}^{(t)}\boldsymbol{\phi}^H-\boldsymbol{\phi}^{(t)}\boldsymbol{\phi}^{(t)H}=\mathbf{\Psi}^{(t)}$$

Hence, we can obtain the conclusion of Lemma 2.

According to Lemma 2, constraint (26b) can be approximated by

$$\tau_j\begin{bmatrix}\widetilde{\mathbf{T}}+\omega_j\mathbf{I} & \widetilde{\mathbf{s}}_j\\ \widetilde{\mathbf{s}}_j^T & F_j-\alpha_j\end{bmatrix}\succeq 0, j\in\mathcal{K}_\mathcal{E} \tag{27}$$

where $\widetilde{\mathbf{T}}=\mathbf{B}_1\otimes\mathbf{\Psi}^{(t)}$, $\widetilde{\mathbf{A}}_{1,j}=\mathbf{B}_1(\mathbf{g}_j\boldsymbol{\phi}^H+\widehat{\overline{\mathbf{G}}}_j^H\mathbf{\Psi}^{(t)})$, $\widetilde{\mathbf{s}}_j=\text{vec}(\widetilde{\mathbf{A}}_{1,\mathrm{j}}^{\mathrm{H}})$, $\widetilde{C}_{1,j}=\text{Tr}\left(\mathbf{g}_\mathrm{j}\mathbf{g}_\mathrm{j}^{\mathrm{H}}\mathbf{B}_1\right)+2\text{Re}\left\{\text{Tr}\left(\mathbf{g}_\mathrm{j}\boldsymbol{\phi}^{\mathrm{H}}\widehat{\overline{\mathbf{G}}}_\mathrm{j}\mathbf{B}_1\right)\right\}+\text{Tr}\left(\widehat{\overline{\mathbf{G}}}_\mathrm{j}^{\mathrm{H}}\mathbf{\Psi}^{(\mathrm{t})}\widehat{\overline{\mathbf{G}}}_\mathrm{j}\mathbf{B}_1\right)$, $F_j=\widetilde{C}_{1,j}-\frac{\eta_1 C_2}{\tau_j K_E}-\frac{\omega_j(\varepsilon_{r,j}^E)^2}{K_E}$.

Similarly, constraint (26c) can be approximated by

$$\begin{bmatrix}\widetilde{\mathbf{T}}_{2,i}+\hat{\omega}_i\mathbf{I} & \widetilde{\mathbf{t}}_i\\ \widetilde{\mathbf{t}}_i^T & \widetilde{C}_{4,i}-\beta_i\end{bmatrix}\succeq 0, i\in\mathcal{K}_\mathcal{I} \tag{28}$$

where $\widetilde{\mathbf{T}}_{2,i}=\overline{\mathbf{B}}_i\otimes\mathbf{\Psi}^{(t)}$, $\widetilde{\mathbf{t}}_i=\text{vec}\left(\widetilde{\mathbf{A}}_{2,\mathrm{i}}^{\mathrm{H}}\overline{\mathbf{B}}_\mathrm{i}^{\mathrm{H}}\right)$, $\widetilde{\mathbf{A}}_{2,i}=\mathbf{h}_i\boldsymbol{\phi}^H+\widehat{\overline{\mathbf{H}}}_i^H\mathbf{\Psi}^{(t)}$, $\widetilde{C}_{4,i}=\text{Tr}[\overline{\mathbf{B}}_\mathrm{i}\widetilde{\mathbf{C}}_3]-\gamma_{\min}\sigma_\mathrm{i}^2-\hat{\omega}_\mathrm{i}(\varepsilon_{\mathrm{r,i}}^{\mathrm{I}})^2$, $\widetilde{\mathbf{C}}_3=\mathbf{h}_i\mathbf{h}_i^H+2\text{Re}\left\{\mathbf{h}_i\boldsymbol{\phi}^H\widehat{\overline{\mathbf{H}}}_i\right\}+\widehat{\overline{\mathbf{H}}}_i^H\mathbf{\Psi}^{(t)}\widehat{\overline{\mathbf{H}}}_i$.

Hence, the subproblem $\mathcal{P}_{1-4-1}$ of optimizing the phase shifts of the RIS can be approximated by

$$\mathcal{P}_{1-4-2} \quad \max_{\boldsymbol{\phi},\boldsymbol{\omega},\hat{\boldsymbol{\omega}},\alpha,\boldsymbol{\beta}} \quad \sum_{j\in\mathcal{K}_\mathcal{E}}\alpha_j+\sum_{i\in\mathcal{K}_\mathcal{I}}\beta_i \tag{29a}$$

$$\text{s.t.} \quad (26\text{d}),(27),(28). \tag{29b}$$

The only non-convex part of Problem $\mathcal{P}_{1-4-2}$ is the unit-modulus constraint for $\boldsymbol{\phi}$ in (26d). Here, the penalty Convex-Concave Procedure (CCP) technique is exploited to transform it into convex constraints. Specifically, the unit-modulus constraint for $\boldsymbol{\phi}$ can be equivalently transformed into $-1\le|\boldsymbol{\phi}_m|^2\le 1$. Furthermore, by introducing the slack variable $\boldsymbol{\rho}=[\rho_1,\cdots,\rho_{2M}]^T$, Problem $\mathcal{P}_{1-4-2}$ can be finally transformed into

$$\mathcal{P}_{1-4-2} \quad \max_{\boldsymbol{\phi},\boldsymbol{\omega},\hat{\boldsymbol{\omega}},\alpha,\boldsymbol{\beta}} \quad \sum_{j\in\mathcal{K}_\mathcal{E}}\alpha_j+\sum_{i\in\mathcal{K}_\mathcal{I}}\beta_i-\kappa^{(t)}\sum_{m=1}^{2M}\rho_m \tag{30a}$$

$$\text{s.t.} \quad \boldsymbol{\omega}\ge 0,\hat{\boldsymbol{\omega}}\ge 0 \tag{30b}$$

$$|\phi_m^{(}t)|^2-2Re(\phi_m^*\phi_m^{(}t))\le\rho_m-1, \quad m\in\mathcal{M} \tag{30c}$$

$$|\phi_m|^2\le 1+\rho_{M+m}, m\in\mathcal{M} \tag{30d}$$

$$(27),(28) \tag{30e}$$

where $\boldsymbol{\rho}=[\rho_1,\ldots,\rho_{2M}]$ is used to relax the unit-modulus constraints, which is also taken as the penalty parts of the objective function. $\kappa^{(t)}$ is used to control the feasibility of the unit-modulus constraints in the tth iteration.

Then, the suboptimal $\boldsymbol{\phi}$ can be obtained by solving Problem $\mathcal{P}_{1-4-2}$ via CVX tool box. Moreover, the overall algorithm for solving original Problem $\mathcal{P}_{1-1}$ is summarized in Algorithm 1.

Algorithm 1 Alternating optimization algorithm for maximizing the total EHE.

1: initialize the iteration number $t=0$, feasible point $\mathbf{w}_i^0$, $\mathbf{v}_j^0$, $\boldsymbol{\phi}^0$, the maximum iteration number T_{max}, convergence tolerance ϵ, $l_\kappa>1$, ζ_1,ζ_2.
2: **Repeat**
3: According to given $\boldsymbol{\phi}^t$, update $\mathbf{w}_i^{(t+1)}$ and $\mathbf{v}_j^{(t+1)}$ by solving Problem $\mathcal{P}_{1-3-3}$; $n=0$, $\boldsymbol{\phi}^n=\boldsymbol{\phi}^t$;
4: **Repeat**
Update $\boldsymbol{\phi}^{(n+1)}$ by solving Problem $\mathcal{P}_{1-4-2}$;
$\kappa^{(n+1)}=max\{l_\kappa\kappa^n,\kappa_{max}\}$;
5: **Until** $\|\boldsymbol{\rho}\|_1\le\zeta_1$ and $\|\boldsymbol{\phi}^{(n+1)}-\boldsymbol{\phi}^n\|_1\le\zeta_2$;
$t=t+1$, $\boldsymbol{\phi}^{(t+1)}=\boldsymbol{\phi}^{(n+1)}$;
6: **Until** $|\frac{\eta_1^{(t+1)}-\eta_1^{(t)}}{\eta_1^{(t)}}|\le\epsilon$.

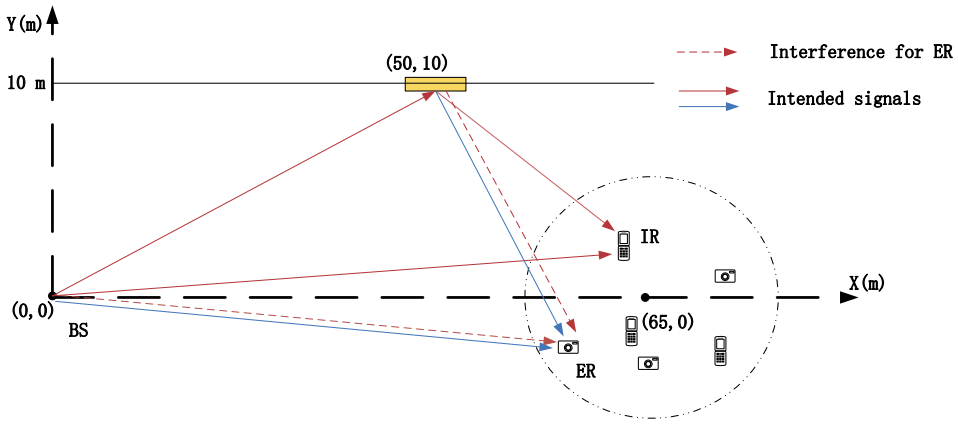

Fig. 2. The simulation model setup.

3.3. Computational complexity

To solve the original Problem $\mathcal{P}_{1-1}$, we decompose it into two subproblems to depart the coupled variables, which still contain SOC and LMIs. Then, the standard interior point method is exploited to solve the approximation form of the subproblems and its general expression complexity is expressed as is firstly reformulated as

$$\mathcal{O}\left(\left(\sum_{j=1}^{J} b_j + 2I\right)^{1/2} n\left(n^2 + n\sum_{j=1}^{J} b_j^2 + \sum_{j=1}^{J} b_j^3 + n\sum_{I=1}^{I} a_i^2\right)\right)$$

where n denotes the number of the optimization variables, J and I are the number of the LMIs of size b_j and a_i, respectively. Hence, the complexity of solving Problem $\mathcal{P}_{1-3-3}$ is $o_{\mathbf{w}_i,\mathbf{v}_j} = \mathcal{O}([K(NM+K+N+1)]^{1/2} n_1[n_1^2 + n_1 K((NM+1)^2 + (K+N)^2)])$ where $n_1 = MK$, and the complexity of solving Problem $\mathcal{P}_{1-4-2}$ is $o_{\boldsymbol{\phi}} = \mathcal{O}([K(NM+1+K)+2M]^{1/2} N[N^2 + NK((NM+1)^2 + K^2)) + MN])$. Therefore, the complexity of the proposed Algorithm 1 that is used for solving the original Problem $\mathcal{P}_{1-1}$ can be denoted as $o_{\mathbf{w}_i,\mathbf{v}_j} + o_{\boldsymbol{\phi}}$ [34].

3.4. Robust beamforming design with non-linear EH model

When ERs exploit non-linear EH model, the total EHE maximization problem is summarized into Problem $\mathcal{P}_2$, which is also difficult to obtain solutions due to the non-convex objective function and the constraints. Nevertheless, we can transform this non-convex problem into its approximation form. By introducing slack variable η_2, Problem $\mathcal{P}_2$ is firstly reformulated as

$$\mathcal{P}_{2-1} \quad \max_{\{\mathbf{w_i}\},\{\mathbf{v_j}\},\boldsymbol{\Phi},\eta_2,\boldsymbol{\beta}} \ \eta_2 \tag{31a}$$

$$\text{s.t.} \quad \sum_{j\in\mathcal{K}_\mathcal{E}} \left(\frac{1}{1+e^{-a_j(\beta_j-b_j)}} - \Omega_j\right)\frac{M_j}{1-\Omega_j} \geq \eta_2\Big(\sum_{i\in\mathcal{K}_\mathcal{I}} \|\mathbf{w}_i\|^2 + \sum_{l\in\mathcal{K}_\mathcal{E}} \|\mathbf{v}_l\|^2 + P_c\Big) \tag{31b}$$

$$\sum_{i\in\mathcal{K}_\mathcal{I}} |\widetilde{\mathbf{g}}_j^H \mathbf{w}_i s_i^I|^2 + \sum_{l\in\mathcal{K}_\mathcal{E}} |\widetilde{\mathbf{g}}_j^H \mathbf{v}_l s_l^E|^2 \geq \beta_j, \quad j\in\mathcal{K}_\mathcal{E} \tag{31c}$$

$$(13\text{b}), (13\text{d}), (21) \tag{31d}$$

where $\boldsymbol{\beta} = [\beta_1, \cdots, \beta_{K_E}]$ denotes the slack optimization variable that is used to control the feasibility of the constraint (31c). Moreover, these constraints include infinitely CSI error constraints and all the variables are coupled to exacerbate the difficulty of solving the problem.

Now, we deal with the constraints (31c), which can be rewritten as

$$\begin{aligned}&\sum_{i\in\mathcal{K}_\mathcal{I}} |\widetilde{\mathbf{g}}_j^H \mathbf{w}_i s_i^I|^2 + \sum_{l\in\mathcal{K}_\mathcal{E}} |\widetilde{\mathbf{g}}_j^H \mathbf{v}_l s_l^E|^2 \geq \beta_j, j\in\mathcal{K}_\mathcal{E}\\ &\Rightarrow C_1 - \beta_j + 2\text{Re}\left\{\text{Tr}(\mathbf{A}_1 \triangle \overline{\mathbf{G}}_j)\right\}\\ &\quad + \boldsymbol{\phi}^H \triangle \overline{\mathbf{G}}_j \mathbf{B}_1 \triangle \overline{\mathbf{G}}_j^H \boldsymbol{\phi} \geq 0, j\in\mathcal{K}_\mathcal{E}\end{aligned} \tag{32}$$

By using Lemma 1, this constraint can be transformed into

$$\begin{bmatrix} \mathbf{T}_0 + \omega_j \mathbf{I} & \mathbf{s}_j \\ \mathbf{s}_j^T & C_1 - \beta_j \end{bmatrix} \succeq 0, j\in\mathcal{K}_\mathcal{E} \tag{33}$$

Hence, the EHE maximization for all the ERs with non-linear EH model in the RIS-aided SWIPT system can be approximated by

$$\mathcal{P}_{2-2} \quad \max_{\{\mathbf{w_i}\},\{\mathbf{v_j}\},\boldsymbol{\Phi},\eta_2,\boldsymbol{\beta}} \ \eta_2 \tag{34a}$$

$$\text{s.t.} \quad (31\text{b}), (31\text{d}), (32) \tag{34b}$$

Note that Problem $\mathcal{P}_{2-2}$ is still very difficult to solve due to the coupled optimization variables. Therefore, AO technique can also be adopted to deal with this non-convex optimization problem and the solving process is the same as that adopted for dealing with Problem $\mathcal{P}_{1-1}$.

4. Simulation results

We investigate the total EHE of all the ERs in the RIS-aided SWIPT system by using the proposed Algorithm 1 under different EH models and system parameters. Specifically, the simulation system model is illustrated in Fig. 2, where one AP is placed at (0 m, 0 m) and the RIS is located at (50 m, 10 m). K_I IRs and K_E ERs are randomly and uniformly distributed in a circle with radius of 5 m, which is centered at (65 m, 0 m). All channels are concerned including large-scale fading and small-scale fading. The large-scale fading model can be illustrated as $\text{PL} = \text{PL}_0 - 10\alpha\log_{10}\left(\frac{d}{d_0}\right)$, where the path loss coefficient is set as α, the reference distance (1 m) is d and the pathloss for the reference distance is denoted as PL_0. The small-scale fading for $\overline{\mathbf{H}}_i, i\in\mathcal{K}_\mathcal{I}$ and $\overline{\mathbf{G}}_j, j\in\mathcal{K}_\mathcal{E}$ is concerned as obeying Raleigh distribution. Hence, the unknown CSI errors of these two channels are respectively modeled as $(\varepsilon_{r,i}^I)^2 = \kappa_H^2 \|vec(\overline{\mathbf{H}}_i)\|_2^2$ and $(\varepsilon_{r,j}^E)^2 = \kappa_G^2 \|vec(\overline{\mathbf{G}}_j)\|_2^2$, where $\kappa_H \in [0,1)$ and $\kappa_G \in [0,1)$ are the coefficients to measure the CSI uncertainties degree. The radii of the uncertainty areas of the bounded CSI error model are modeled as [34]

$$\xi_{r,i} = \sqrt{\frac{(\varepsilon_{r,i}^I)^2}{2} F_{2MN}^{-1}(1-\rho)}, i\in\mathcal{K}_\mathcal{I}$$

and

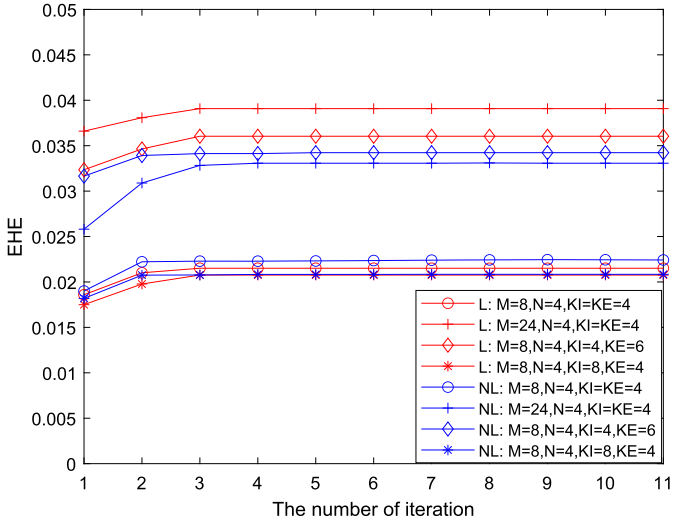

Fig. 3. The convergence of the proposed algorithm for the RIS-aided SWIPT system.

$$\xi_{r,j} = \sqrt{\frac{(\varepsilon_{r,j}^{E})^2}{2} F_{2MN}^{-1}(1-\rho)}, j \in \mathcal{K}_{\mathcal{E}}$$

where $F_{2NM}^{-1}(\cdot)$ denotes the inverse cumulative distribution function of Chi-square distribution with degrees of freedom $2NM$. $\rho = 0.05$ is the outage probability.

The parameters of the non-linear EH model are chosen as $M_j = 24$ mW, $a_j = 1500$ and $b_j = 0.0014, j \in \mathcal{K}_{\mathcal{E}}$ [33]. Here, we set the minimum SINR requirement of each IR as $\gamma_{min} = 1$ dB, the noise power as $\sigma_j^2 = -174$ dBm, the maximum transmit power of the AP as $P_{max} = 25$ dBm. The circuits power consumption as $P_c = 10$ dBm, the channel uncertainty is chosen as $\varepsilon_{r,i}^{I} = \varepsilon_{r,j}^{E} = 0.02, i \in \mathcal{K}_{\mathcal{I}}, j \in \mathcal{K}_{\mathcal{E}}$.

Fig. 3 shows the convergence behavior of the proposed Algorithm 1 in the RIS-aided SWIPT system with different system parameters and EH models for all the ERs. Simulation results demonstrate that the proposed algorithm converges very fast and keeps stable within several iterations. Furthermore, it also shows that ERs have better EHE with linear EH model than that with non-linear EH model. This is mainly because the linear EH model just investigates EH of all ERs under ideal conditions, which ignore some inevitable interferences like phase offsets, frequency and non-linear power amplifiers.

Fig. 4 compares the average Central Processing Unit (CPU) processing time of the proposed algorithms versus the numbers of reflection elements at RIS, antennas at AP, the numbers of IRs and ERs. The results are obtained by using a computer with a 2.3 GHz i7-11800H CPU and 16 GB RAM. The simulation results show that the robust algorithm with linear EH model requires much less processing time than that with non-linear EH model. This is due to the fact that there are some large-dimensional LMIs in the optimization problem when the non-linear EH is adopted, which increases the computational complexity of the proposed robust algorithm. Moreover, it is observed that the number of the antennas at AP and the reflecting elements at RIS have crucial influence on the CPU processing time, especially when those numbers become larger.

Fig. 5 presents the maximum transmit power of the AP versus the total EHE of all ERs under different system parameters in the RIS-aided SWIPT system with linear and non-linear EH models, respectively. It is observed that the total EHE increases with the growth of the maximum transmit power of AP both in the linear and the non-linear EH models. It also shows that, no matter what kind of EH model is used for all ERs, the growth trend of the total EHE will slow down even when the maximum transmit power of AP increases. But when the number of the RIS's elements increases from 8 to 12, the total EHE still increases very fast both in the linear and non-linear EH models, demonstrating the

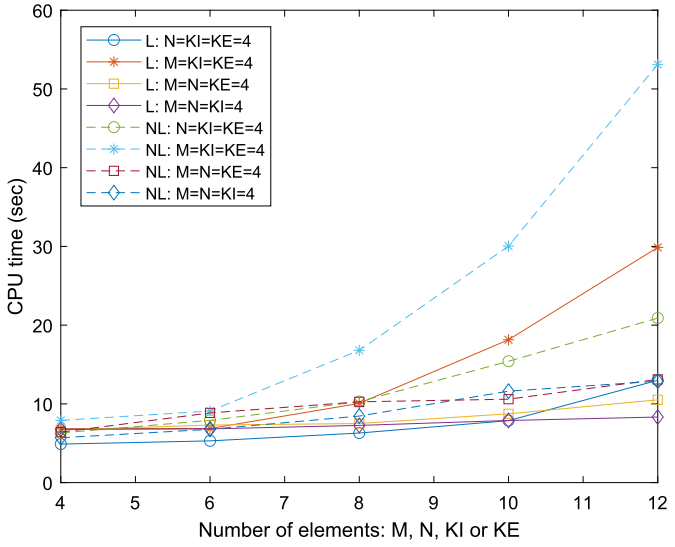

Fig. 4. Average CPU processing time versus the number of the elements of RIS, antennas of AP, the number of IRs and the ERs.

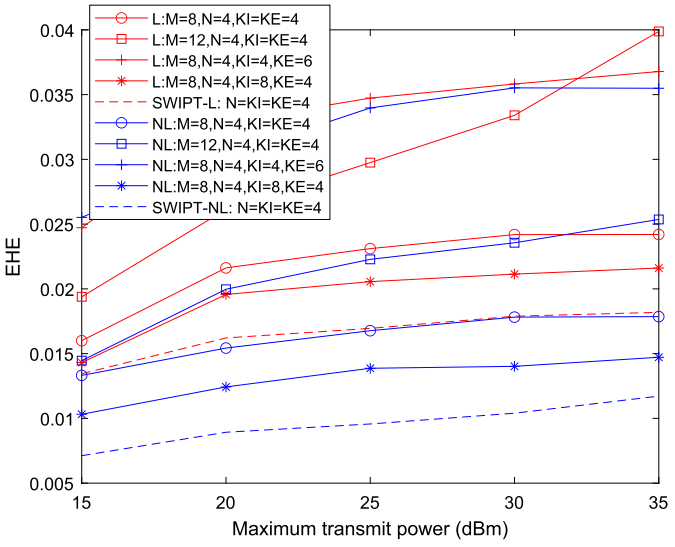

Fig. 5. Transmit power versus EHE with linear and non-linear EH models for the RIS-aided SWIPT system.

effectiveness of deploying the RIS to aid the EH process for ERs in the SWIPT system. Because the non-linear EH model can characterize the behavior of various practical EH circuits, the total EHE with non-linear EH model under the same maximum transmit power of AP is lower than that with linear EH model. Furthermore, it is observed that the EHE of the system can be improved with the help of RIS no matter what kinds of EH model is used in SWIPT.

Fig. 6 shows the total EHE versus the number of reflecting elements of RIS under different EH models and the system parameters. It is seen that the total EHE of all ERs increases with the number of RIS's reflecting elements no matter what kind of EH models is used for ERs. Furthermore, when the reflecting elements of RIS increase, the growth of the total EHE is much more noticeable in the non-linear EH model compared to the linear EH model. This discrepancy becomes more prominent as the number of the reflecting elements of RIS increases. These results demonstrate the loss of the total EHE of all the ERs that is caused by EH models and the uncertainty CSI errors can be compensated by deploying the RIS with massive number of reflecting elements.

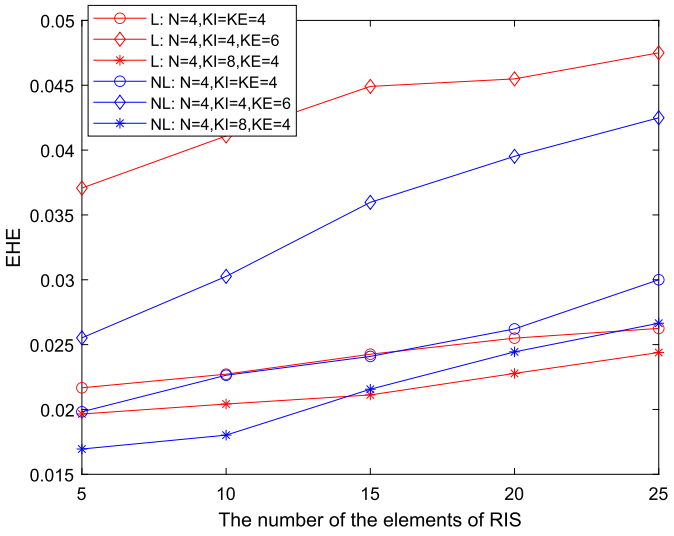

Fig. 6. The number of RIS's elements versus EHE for RIS-aided SWIPT system.

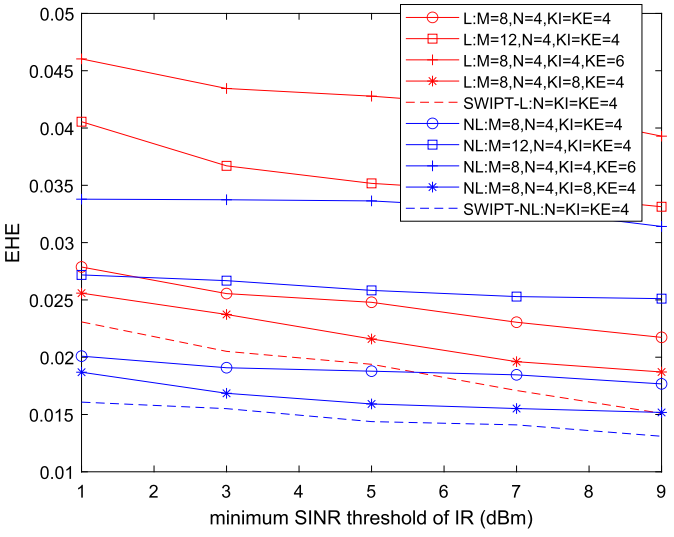

Fig. 7. Minimum SINR threshold of IR versus EHE for RIS-aided SWIPT system.

Fig. 7 illustrates the total EHE of all ERs versus the minimum SINR requirements for all IRs. It is known that the total EHE decreases with the increase of the minimum SINR threshold of IRs both under the linear and non-linear EH models. In addition, it is also observed that the increase of the number of IR decreases the total EHE of all ERs. This is primarily because, to increase the number of IRs, more transmit power is required to meet the minimum SINR requirement for all IRs, thereby reducing the transmit power used for the ERs' EH process. Moreover, the findings also demonstrate that the EHE of the RIS-assisted SWIPT can be enhanced to a certain extent even when the SINR threshold of IRs increases.

5. Conclusions

We proposed robust beamforming design for the total EHE maximization under both the linear and non-linear EH models in the RIS-aided SWIPT system. The purpose of this paper is to maximize the total EHE of all ERs with respect to the minimum SINR requirement for all IRs, the maximum transmit power of AP and the unit-modulus of the RIS's reflecting elements. These non-convex problems are departed into two approximation subproblems and the constraints contained CSI errors are approximated using the S-procedure. Then, the reformulated problems were solved by using AO technique. It is shown that the overall EHE performance of all ERs under the linear EH model is superior to that under the non-linear model. Moreover, the increase of the number of reflecting elements can effectively improve the total EHE of all ERs, regardless of the EH models involved.

CRediT authorship contribution statement

Xingquan Li: Writing – original draft. **Hongxia Zheng:** Methodology. **Chunlong He:** Formal analysis. **Xiaowen Tian:** Formal analysis. **Xin Lin:** Formal analysis.

Declaration of competing interest

The authors declare that they have no known competing financial interests or personal relationships that could have appeared to influence the work reported in this paper.

Acknowledgements

This work is supported by the Shenzhen Basic Research Program under Grant JCYJ20220531103008018, 20231120142345001, 20200812112423002, Shenzhen Stability Support Project under Grant 20231127144045001 and the Double Height Construction under Grant SZIIT2022KJ023.

References

[1] E. Sisinni, A. Saifullah, S. Han, U. Jennehag, M. Gidlund, Industrial internet of things: challenges, opportunities, and directions, IEEE Trans. Ind. Inform. 14 (11) (2018) 4724–4734.
[2] H. Lasi, P. Fettke, H.-G. Kemper, T. Feld, M. Hoffmann, Industry 4.0, Bus. Inf. Syst. Eng. 6 (4) (2014) 239–242.
[3] W. Qin, S. Chen, M. Peng, Recent advances in industrial internet: insights and challenges, Digit. Commun. Netw. 6 (1) (2020) 1–13.
[4] W. Mao, Z. Zhao, Z. Chang, G. Min, W. Gao, Energy-efficient industrial internet of things: overview and open issues, IEEE Trans. Ind. Inform. 17 (11) (2021).
[5] G. Dileep, A survey on smart grid technologies and applications, Renew. Energy 146 (2020) 2589–2625.
[6] S.S. Hajam, S.A. Sofi, IoT-fog architectures in smart city applications: a survey, China Commun. 18 (11) (2021) 117–140.
[7] S. Misra, P.K. Bishoyi, S. Sarkar, I-MAC: in-body sensor MAC in wireless body area networks for healthcare IoT, IEEE Syst. J. 15 (3) (2021) 4413–4420.
[8] B.M. Lee, H. Yang, Energy-efficient massive MIMO in massive industrial internet of things networks, IEEE Int. Things J. 9 (5) (2022) 3657–3671.
[9] W. Saad, M. Bennis, M. Chen, A vision of 6G wireless systems: applications, trends, technologies, and open research problems, IEEE Netw. 34 (3) (2020) 134–142.
[10] L. Chettri, R. Bera, A comprehensive survey on internet of things (IoT) toward 5G wireless systems, IEEE Int. Things J. 7 (1) (2020) 16–32.
[11] C. Guo, J. Xin, L. Zhao, X. Chu, Performance analysis of cooperative NOMA with energy harvesting in multi-cell networks, China Commun. 16 (11) (2019) 120–129.
[12] I. Krikidis, S. Timotheou, S. Nikolaou, G. Zheng, D.W.K. Ng, R. Schober, Simultaneous wireless information and power transfer in modern communication systems, IEEE Commun. Mag. 52 (11) (2014) 104–110.
[13] W. Lu, P. Si, G. Huang, L. Qian, N. Zhao, Y. Gong, SWIPT cooperative spectrum sharing for 6G-enabled cognitive IoT network, IEEE Int. Things J. 8 (20) (2021) 15070–15080.
[14] P.V. Tuan, I. Koo, Optimizing efficient energy transmission on a SWIPT interference channel under linear/nonlinear EH models, IEEE Syst. J. 14 (1) (2020) 457–468.
[15] J. Huang, C.-C. Xing, M. Guizani, Power allocation for D2D communications with SWIPT, IEEE Trans. Wirel. Commun. 19 (4) (2020) 2308–2320.
[16] C. Pan, H. Ren, K. Wang, J. Kolb, M. Elkashlan, M. Chen, M. Renzo, Y. Hao, J. Wang, A. Swidlehurst, X. You, L. Hanzo, Reconfigurable intelligent surfaces for 6G systems: principles, applications, and research directions, IEEE Commun. Mag. 59 (6) (2021) 14–20.
[17] C. Pan, H. Ren, K. Wang, W. Xu, M. Elkashlan, A. Nallanathan, L. Hanzo, Multicell MIMO communications relying on intelligent reflecting surface, IEEE Trans. Wirel. Commun. 119 (8) (2020) 5218–5233.
[18] S. Hu, Z. Wei, Y. Cai, C. Liu, D.W.K. Ng, J. Yuan, Robust and secure sum-rate maximization for multiuser MISO downlink systems with self-sustainable IRS, IEEE Trans. Commun. 69 (10) (2021) 7032–7049.
[19] C. Pan, H. Ren, K. Wang, M. Elkashlan, A. Nallanathan, J. Wang, L. Hanzo, Intelligent reflecting surface aided MIMO broadcasting for simultaneous wireless information and power transfer, IEEE J. Sel. Areas Commun. 38 (8) (2020) 1719–1734.

[20] K. Zhi, C. Pan, H. Ren, K.K. Chai, M. Elkashlan, Active RIS versus passive RIS: which is superior with the same power budget?, IEEE Commun. Lett. 26 (5) (2022) 1150–1154.
[21] S. Ma, W. Shen, X. Gao, J. An, Robust channel estimation for RIS-aided millimeter-wave system with RIS blockage, IEEE Trans. Veh. Technol. 71 (5) (2022) 5621–5626.
[22] S. Arzykulov, G. Nauryzbayev, A. Celik, A.M. Eltawil, RIS-assisted full-duplex relay systems, IEEE Syst. J. 16 (4) (2022) 5729–5740.
[23] J. An, C. Xu, L. Gan, L. Hanzo, Low-complexity channel estimation and passive beamforming for RIS-assisted MIMO systems relying on discrete phase shifts, IEEE Trans. Commun. 70 (2) (2022) 1245–1260.
[24] X. Peng, P. Wu, H. Tan, M. Xia, Optimization for IRS-assisted MIMO-OFDM SWIPT system with nonlinear EH model, IEEE Int. Things J. 9 (24) (2022) 25253–25268.
[25] M. Diamanti, E.E. Tsiropoulou, S. Papavassiliou, The joint power of NOMA and reconfigurable intelligent surfaces in SWIPT networks, in: Proceedings of the 2021 IEEE 22nd International Workshop on Signal Processing Advances in Wireless Communications, 2021, pp. 621–625.
[26] H. Ren, Z. Chen, G. Hu, Z. Peng, C. Pan, J. Wang, Transmission design for active RIS-aided simultaneous wireless information and power transfer, IEEE Wirel. Commun. Lett. 12 (4) (2023) 600–604.
[27] Q. Wu, R. Zhang, Joint active and passive beamforming optimization for intelligent reflecting surface assisted SWIPT under QoS constraints, IEEE J. Sel. Areas Commun. 38 (8) (2020) 1735–1748.
[28] J. Liu, K. Xiong, Y. Lu, D.W.K. Ng, Z. Zhong, Z. Han, Energy efficiency in secure IRS-aided SWIPT, IEEE Wirel. Commun. Lett. 9 (11) (2020) 1884–1888.
[29] R. Zhang, K. Xiong, Y. Lu, P. Fan, D.W.K. Ng, K.B. Letaief, Energy efficiency maximization in RIS-assisted SWIPT networks with RSMA: a PPO-based approach, IEEE J. Sel. Areas Commun. 41 (5) (2023) 1413–1430.
[30] S. Zargari, A. Khalili, R. Zhang, Energy efficiency maximization via joint active and passive beamforming design for multiuser MISO IRS-aided SWIPT, IEEE Wirel. Commun. Lett. 10 (3) (2021) 557–561.
[31] D.W.K. Ng, E.S. Lo, R. Schober, Multiobjective resource allocation for secure communication in cognitive radio networks with wireless information and power transfer, IEEE Trans. Veh. Technol. 65 (5) (2016) 3166–3184.
[32] M. Sheng, L. Wang, X. Wang, Y. Zhang, C. Xu, J. Li, Energy efficient beamforming in MISO heterogeneous cellular networks with wireless information and power transfer, IEEE J. Sel. Areas Commun. 34 (4) (2016) 954–968.
[33] S. Jang, H. Lee, S. Kang, T. Oh, I. Lee, Energy efficient SWIPT systems in multi-cell MISO networks, IEEE Trans. Wirel. Commun. 17 (12) (2018) 8180–8194.
[34] G. Zhou, C. Pan, H. Ren, K. Wang, A. Nallanathan, A framework of robust transmission design for IRS-aided MISO communications with imperfect cascaded channels, IEEE Trans. Signal Process. 68 (2020) 5092–5106.
[35] H. Zheng, C. Pan, C. Zhang, X. Li, C. He, Y. Yang, M. Dai, Robust transmission design for RIS-aided wireless communication with both imperfect CSI and transceiver hardware impairments, IEEE Int. Things J. 10 (5) (2023) 4621–4635.
[36] S. Boyd, L.G. El, E. Ferron, V. Balakrishnan, Linear Matrix Inequalities in System and Control Theory, Philadelphia, 1994.
[37] Z. Szabó, Z. Biró, J. Bokor, Multivariate S-procedure, in: Proceedings of the 2013 European Control Conference, 2013, pp. 3907–3912.